Rheological behaviour of different composite materials for additive manufacturing of 3D bone scaffolds

DOI:
10.1016/j.jmrt.2023.03.231

Document Version
Final published version

Available online at www.sciencedirect.com

jmr&t Journal of Materials Research and Technology

journal homepage: www.elsevier.com/locate/jmrt

Original Article

Rheological behaviour of different composite materials for additive manufacturing of 3D bone scaffolds

Evangelos Daskalakis [a,*], *Mohamed H. Hassan* [a], *Abdalla M. Omar* [a], *Glen Cooper* [a], *Andrew Weightman* [a], *Paulo Bartolo* [a,b,**]

[a] *School of Mechanical, Aerospace and Civil Engineering, University of Manchester, Manchester, M13 9PL, UK*
[b] *Singapore Centre for 3D Printing, School of Mechanical and Aerospace Engineering, Nanyang Technological University, 639798 Singapore*

ARTICLE INFO

Article history:
Received 5 December 2022
Accepted 31 March 2023
Available online 6 April 2023

Keywords:
Additive manufacturing
Polymer-ceramic blends
Printability
Rheology

ABSTRACT

The production of scaffolds for bone tissue applications is requiring a combination of physical and biological properties, which are depending on the materials morphology and pro-cessing conditions during the production process. The aim of the paper is the investigation of rheological behaviour of polymer and composite blends regularly used for the production of scaffolds for bone tissue applications with the use of additive manufacturing. Poly-ε-caprolactone (PCL), hydroxyapatite (HA), β-tri-calcium phosphate (TCP) and Bioglass 45S5 blends containing different ceramic concentrations (10 wt%, 15 wt% and 20 wt%) were prepared with the use of melt blending procedure and investigated with the use of oscillation and rotational rheology tests. Results are showing that all blends are presenting viscoelastic behaviour with higher viscous modulus, compared with elastic modulus for low frequencies, with this difference reducing while the frequency is increasing. All blends are presenting shear-thinning behaviour suitable for use with additive manufacturing methods. Viscous and elastic modulus are increasing by adding ceramic particles. Results are presenting that PCL/HA blends of the same material concentration are presenting higher elastic modulus properties compared with the other blends, while PCL/Bioglass blends are presenting lower loss factor, lower relaxation time and lower shear viscosity making them easier to handle during the printing procedure.

* Corresponding author. School of Mechanical, Aerospace and Civil Engineering, University of Manchester, Manchester, M13 9PL, United Kingdom.
** Corresponding author. Singapore Centre for 3D Printing, School of Mechanical and Aerospace Engineering, Nanyang Technological University, 639798 Singapore.
E-mail addresses: evangelos.daskalakis@manchester.ac.uk (E. Daskalakis), mohamed.hassan@manchester.ac.uk (M.H. Hassan), abdalla.omar@manchester.ac.uk (A.M. Omar), glen.cooper@manchester.ac.uk (G. Cooper), weightman@manchester.ac.uk (A. Weightman), pbartolo@ntu.edu.sg (P. Bartolo).
https://doi.org/10.1016/j.jmrt.2023.03.231

1. Introduction

Additive manufactured scaffolds represent the most suitable approach for tissue engineering applications [1–6]. Different additive manufacturing techniques such as vat-photopolymerization, binder jetting, powder bed fusion and extrusion-based systems have been used to create scaffolds with well-defined architecture, pore shape, pore size, pore distribution, pore interconnectivity and porosity [7–14]. Among these techniques extrusion-based processes are the most commonly used additive manufacturing for the fabrication of bone scaffolds [15–19]. Extrusion-based additive manufacturing is based on melting a polymer-based material and printing the molten material in a moveable platform where the material will cool down. During this heating a cooling process there is an inherent morphological development process that will determine the final properties of the printed scaffolds [20–26]. The kinetics of the cooling process also determine the crystalline structure formation (e.g., degree of crystallinity and crystal size) and volumetric changes of the printed filaments [27–31]. The heating process, which depends on the material to be printed, determines the viscosity of the printed material, how easy is the material printed and the shape fidelity of the printed part upon cooling. To guarantee good printability, materials must present a shear thinning behaviour that describes a material in which the viscosity decreases by increasing the shear rate [31–36].

Materials for extrusion-based additive manufacturing can be in the form of pellets, processed through screw-assisted extrusion systems, or in the form of filaments, processed through filament-based extrusion systems also known as Fused Deposition Modelling (FDM) systems [37,38]. Most studies on bone scaffolds are based on the use of screw-assisted extrusion additive manufacturing [39,40].

Scaffolds can be made with bioceramic materials, but such scaffolds are usually brittle, or using biodegradable and biocompatible polymers, but usually these scaffolds present limited bioactivity [41–43] 412–414]. These limitations can be addressed through the use of polymer/ceramic composite blends. PCL is one of the most commonly used polymeric material for bone tissue engineering applications [44,45] 415, 416]. It is biocompatible, biodegradable, easy to process, but presents limited mechanical properties, low bioactivity and long degradation times [46,47]. To overcome these limitations, PCL is usually combined with bioactive ceramics such as HA, TCP and Bioglass [48–52]. These reinforcements have the potential to increase the overall mechanical properties of the 3D printed composite scaffolds and also cell attachment, proliferation and differentiation. However, the addition of bioceramic particles have also a strong effect on the rheological properties of the blends compromising their printability and eventually clogging the printing head.

This Chapter investigates the effect of different reinforcements (hydroxyapatite, β-tricalcium phosphate and Bioglass 45S5) and level of reinforcement (0 wt%, 10 wt%, 15 wt % and 20 wt%) on the rheological and viscoelastic properties of the materials.

2. Materials and methods

2.1. Materials and methods

Poly-ε-caprolactone (PCL) (melting point = 60 °C, glass transition temperature = −60 °C, molecular weight = 50000Da, CAPA 6500, Perstorp Caprolactones, Cheshire, UK) in pellet shape. Hydroxyapatite (HA) (molecular weight = 502.31 gr/mol, melting point = 1100 °C, Sigma-Aldrich, St. Louis, USA) in nanopowder shape (<20 nm particle size), β-tricalcium phosphate (TCP) (molecular weight = 310.18 gr/mol, melting point = 1391 °C, Sigma-Aldrich, St. Louis, USA) in powder shape (ranging between 20 μm and 30 μm) and Bioglass 45S5 (6 wt% P_2O_5, 45 wt% SiO_2, 24.5 wt% Na2O and 24.5 wt% CaO, CeraDynamics Ltd. James Kent Group, Stoke, UK), in powder shape (<10 μm particles size) (Table 1).

2.2. Morphological analysis

Scanning electron microscopy (SEM) images were taken using FEI Quanta 200 (FEI ESEM Quanta 200, FEI Company, Hillsboro, Orlando, USA) to investigate the morphology of HA, TCP and Bioglass 45S5 particles in powder form. EMITECH K550X sputter coater (Quorum Technologies, Laughton, East Sussex, UK) was used to coat the powder particles (platinum coating).

2.3. Rheology analysis

Rheological analysis including oscillation and rotational studies were investigated with the use of DHR-3 TA Instrument (TA Instruments, New Castle, UK). The materials were tested using a 20 mm (diameter) steel parallel plate with a gap distance of 450 μm. Three samples of each blend were used, and three different temperatures were considered for the rheology tests: 80 °C, 90 °C and 100 °C, which are within a typical printing temperature range for screw-assisted extrusion-based 3D printing of PCL scaffolds. To simulate the molten state during the printing process, the materials were preheated for 15 min. For the oscillation test a constant strain rate of 1% was considered, while the frequency of logarithmic sweep was between 10 HZ and 0.01 Hz. For the rotational test the shear rate of the logarithmic sweep was between $0.01s^{-1}$ and $100s^{1}$. The results presented in this research are the average values of the three samples of each blend.

The measurement of the storage modulus (G′) and loss modulus (G″), which describes the elastic and viscous

Table 1 – Composition of the different material blends (values are in wt%).

Material /Configuration	PCL	PCL/HA	PCL/TCP	PCL/Bioglass
0 wt%	100	–	–	–
10 wt%	–	90/10	90/10	90/10
15 wt%	–	85/15	85/15	85/15
20 wt%	–	80/20	80/20	80/20

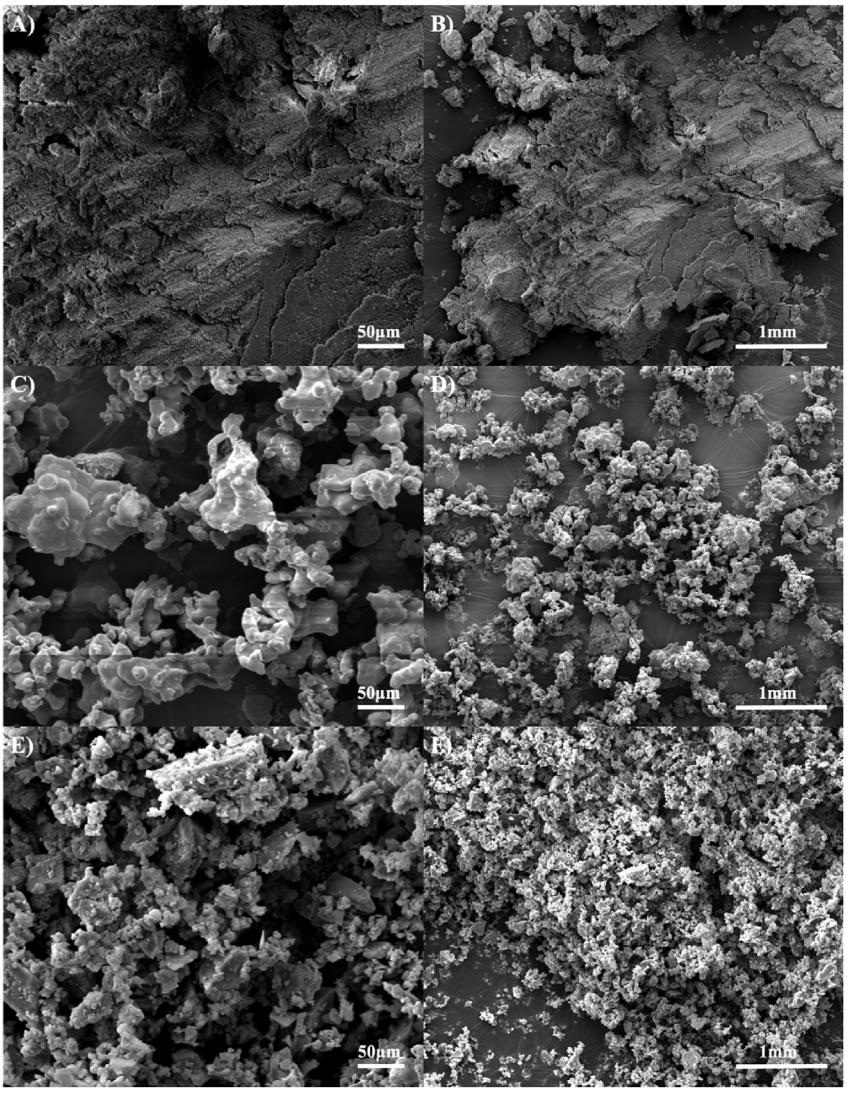

Fig. 1 – SEM images of A) and B) HA nanoparticles, C) and D) TCP microparticles and E) and F) Bioglass microparticles.

behaviour of the material respectively, allows to evaluate the viscoelastic characteristics of the considered blends. Storage modulus and loss modulus are given by the following equations [53]:

$$G' = (\sigma_o / \gamma_o)\cos\delta \quad (1)$$

$$G'' = (\sigma_o / \gamma_o)\sin\delta \quad (2)$$

where σ_o is the stress amplitude, γ_o is the strain amplitude and δ is the phase angle between 0° and 90°.

To investigate the average the ratio of energy dissipated to the maximum energy stored it is important to determine the ratio of the average power loss to the peak load loss by calculating the loss factor (tanδ) [53]:

$$\tan\delta = G'/G'' \quad (3)$$

Accelerated degradation studies were conducted using sodium hydroxide (NaOH) of 5 mol/l (5 N) in aqueous solution (VWR, Pennsylvania, USA), with a density of 1.185 gr/cm3 (20 °C), solubility of 20 °C and 14 pH (H2O, 20 °C). The degradation period took place for 5 days. On each day, 5 samples were used from each considered case and measured using a high precision balance. At each time point, the samples were removed from the NaOH and washed three times with the use of deionised water and left to dry overnight. Once completely dried the samples were measured to determine the weight reduction. The amount of NaOH used for 5 rectangular scaffolds was 15 ml and for 5 the anatomically designed bone bricks was 50 ml (due to their size). The pH was monitoring throughout the experimental work and no changes were observed (pH of 14).

$$\tau = \eta\dot{\gamma}^n \quad (4)$$

where τ is the shear stress (Pa), η is the flow consistency or coefficient (Pa.sn), "$\dot{\gamma}$" is the shear rate (s^{-1}) and n is the power law index that defines the material behaviour [54].

n < 1: shear-thinning material

n = 1: Newtonian material

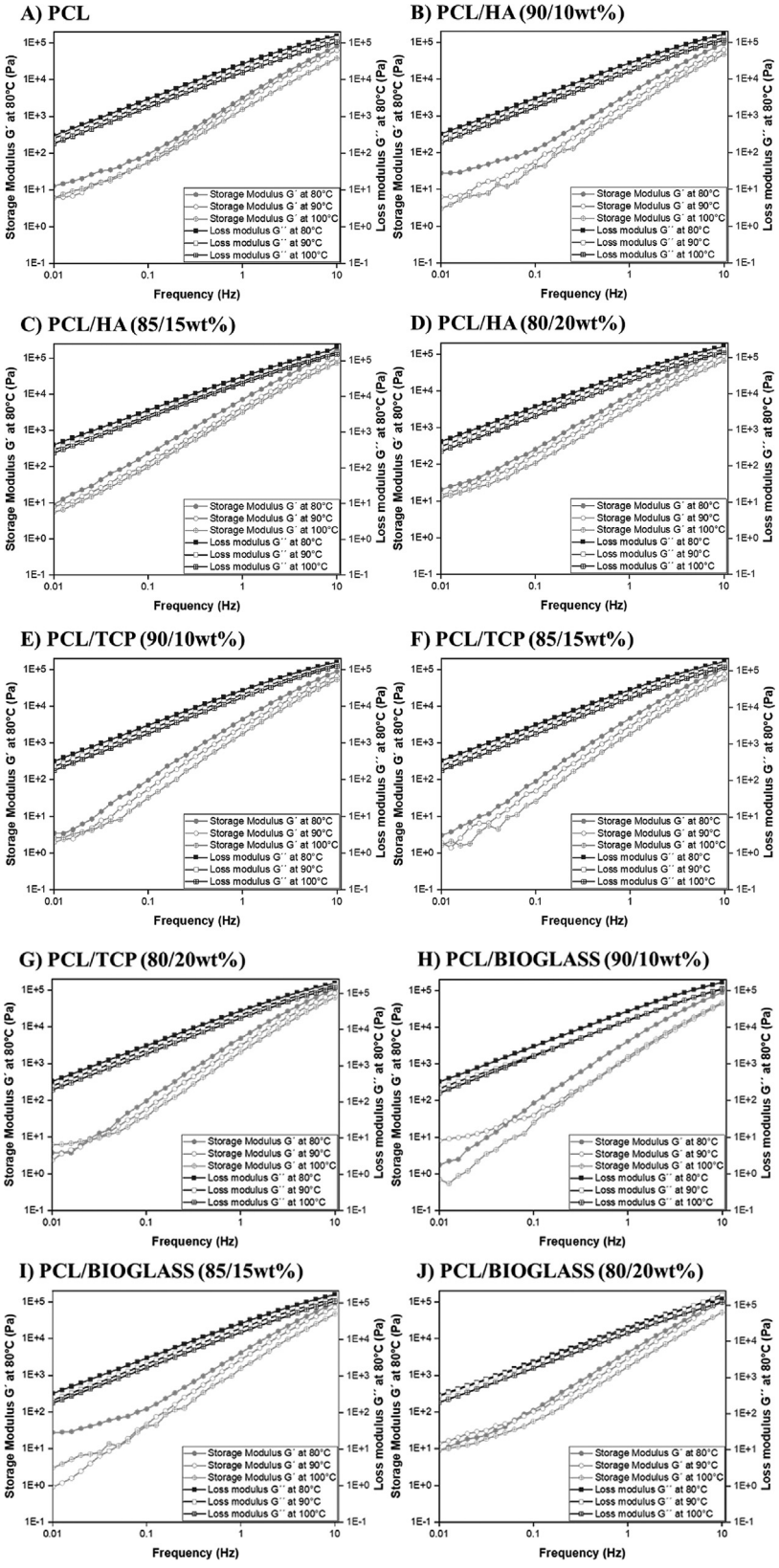

Fig. 2 – Frequency as a function of storage modulus and loss modulus for the same material concentration at different temperatures of A) PCL, B) PCL/HA (90/10 wt%), C) PCL/HA (85/15 wt%), D) PCL/HA (80/20 wt%), E) PCL/TCP (90/10 wt%), F) PCL/TCP (85/15 wt%), G) PCL/TCP (80/20 wt%), H) PCL/Bioglass (90/10 wt%), I) PCL/Bioglass (85/15 wt%) and J) PCL/Bioglass (80/20 wt%).

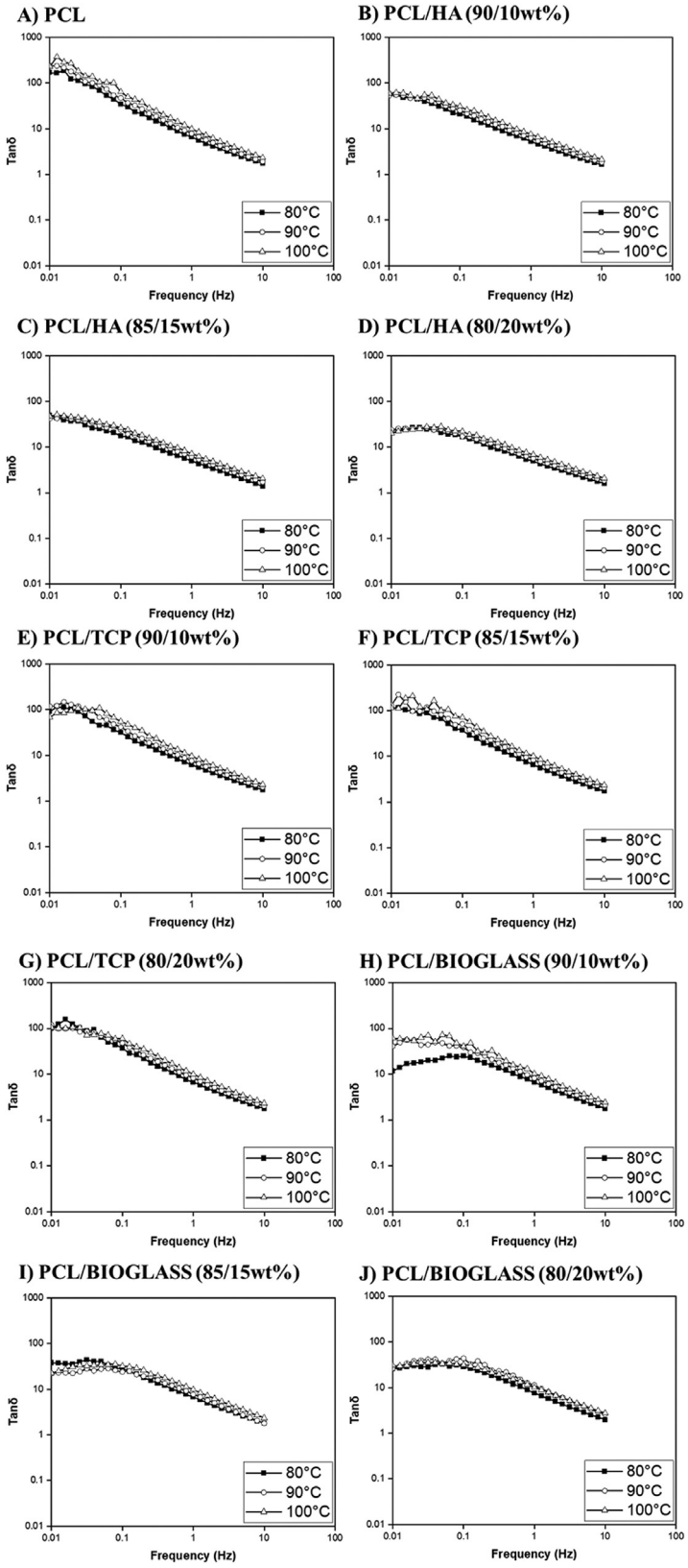

Fig. 3 – Frequency as a function of Loss factor for the same material concentration at different temperatures of A) PCL, B) PCL/HA (90/10 wt%), C) PCL/HA (85/15 wt%), D) PCL/HA (80/20 wt%), E) PCL/TCP (90/10 wt%), F) PCL/TCP (85/15 wt%), G) PCL/TCP (80/20 wt%), H) PCL/Bioglass (90/10 wt%), I) PCL/Bioglass (85/15 wt%) and J) PCL/Bioglass (80/20 wt%).

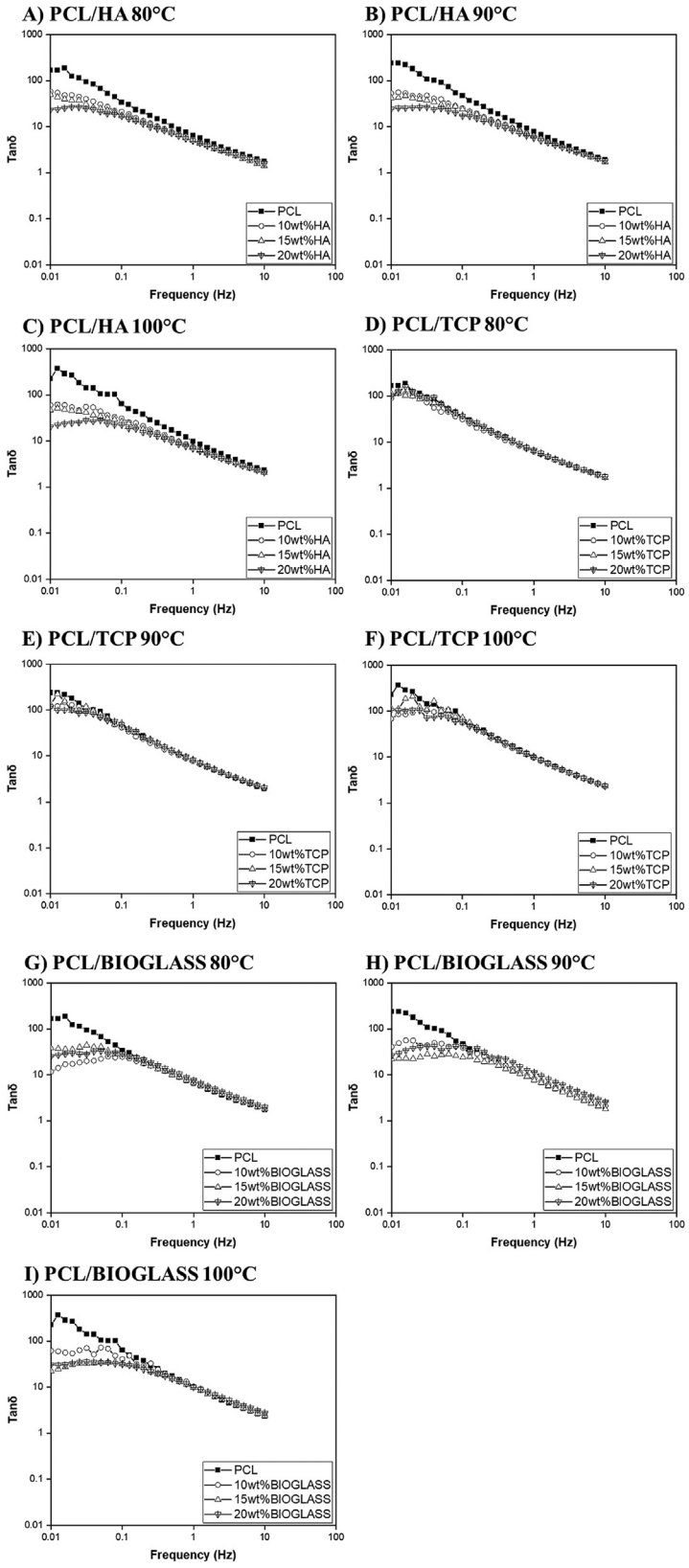

Fig. 4 – Frequency as a function of Loss factor for the same material content of A) PCL/HA (90/10 wt%), B) PCL/HA (85/15 wt%), C) PCL/HA (80/20 wt%), D) PCL/TCP (90/10 wt%), E) PCL/TCP (85/15 wt%), F) PCL/TCP (80/20 wt%), G) PCL/Bioglass (90/10 wt%), H) PCL/Bioglass (85/15 wt%) and I) PCL/Bioglass (80/20 wt%).

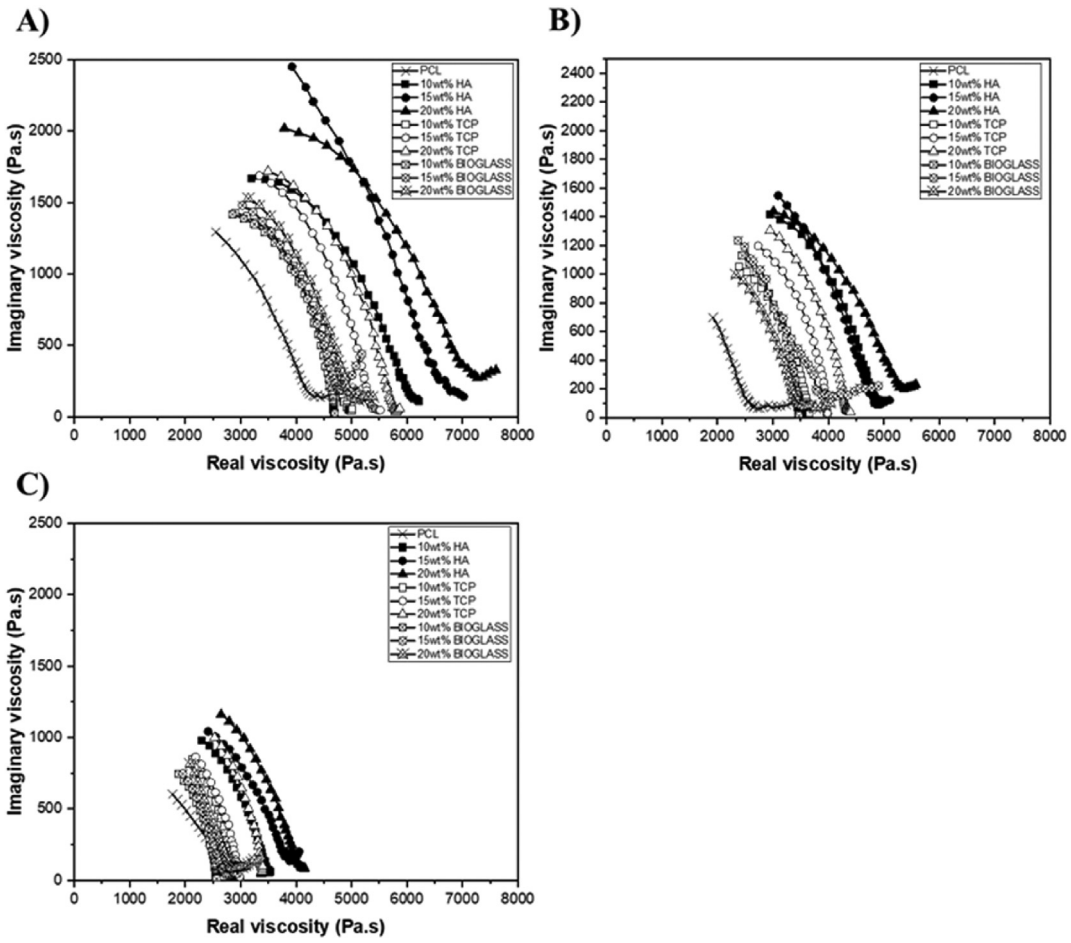

Fig. 5 – Cole-Cole plot of real viscosity as a function of imaginary viscosity for all material contents of A) 80 °C, B) 90 °C and C) 100 °C.

n > 1: shear-thickening material.

Moreover, to investigate the homogeneity dispersion of the materials in the blends, the Cole-Cole plot was used considering both the imaginary viscosity and the real viscosity [54]:

$$\eta'' = G'/w \quad (5)$$

$$\eta' = G''/w \quad (6)$$

where η'' is the imaginary viscosity, η' the real viscosity and w is the oscillation frequency.

3. Results and discussion

3.1. *Morphological analysis*

Fig. 1 presents the ceramic materials used for the production of PCL/HA, PCL/TCP and PCL/Bioglass blends for the rheological tests.

3.2. *Oscillation analysis*

Fig. 2 shows both the storage and the loss modulus for all considered material compositions at different temperatures (80 °C, 90 °C and 100 °C) as a function of frequency. As observed, both storage modulus and loss modulus increase by increasing the frequency from 0.01 Hz to 10 Hz. This can be due to a sufficient relaxation time of polymer chains at low frequency allowing the self-disentanglement [55–64]. Moreover, it can be observed that, for all material compositions, the loss modulus is higher than the storage modulus, indicating that the viscous behaviour is the dominant effect within this

Table 2 – Zero shear viscosity (Pa.s) results of polymer blends at different temperatures.

Temperature/Material Composition	80 °C	90 °C	100 °C
PCL	2922.4	2335.4	1766
PCL/HA (90/10 wt%)	3671.4	2699.1	2140.6
PCL/HA (85/15 wt%)	4174	2895.9	2462.7
PCL/HA (80/20 wt%)	4250.4	3038.4	2438.6
PCL/TCP (90/10 wt%)	3113.1	2473.3	2034.8
PCL/TCP (85/15 wt%)	3610.8	2617.1	2183.1
PCL/TCP (80/20 wt%)	3908.6	3165.3	2538.7
PCL/Bioglass (90/10 wt%)	3267.3	2438.1	1970.8
PCL/Bioglass (85/15 wt%)	3362.9	2480.2	1843.9
PCL/Bioglass (80/20 wt%)	3445.5	2950	1975

Table 3 – Relaxation time (s) results of polymer blends at different temperatures.

Temperature/Material Composition	80 °C	90 °C	100 °C
PCL	0.0011	0.0005	0.0003
PCL/HA (90/10 wt%)	0.0022	0.0021	0.001
PCL/HA (85/15 wt%)	0.0026	0.0023	0.0014
PCL/HA (80/20 wt%)	0.0045	0.0036	0.0016
PCL/TCP (90/10 wt%)	0.0011	0.0004	0.0002
PCL/TCP (85/15 wt%)	0.0011	0.0006	0.0003
PCL/TCP (80/20 wt%)	0.0012	0.0009	0.0003
PCL/Bioglass (90/10 wt%)	0.0008	0.0006	0.0004
PCL/Bioglass (85/15 wt%)	0.0012	0.0006	0.0004
PCL/Bioglass (80/20 wt%)	0.0013	0.0007	0.0007

temperature range, indicating that 3D printing is a suitable technique to process these blends. Additionally, by increasing the frequency it is possible to observe that the difference between storage modulus and loss modulus decreases, suggesting that composite materials present a more solid-like behaviour at a high deformation rate, which may hinder the flowability of the materials during the printing process. Furthermore, results show that the addition of ceramics into the PCL matrix decreases the storage modulus compared with pure PCL, while loss modulus does not show any significant differences. On the other hand, blends containing PCL/HA (80/20 wt%) and PCL/Bioglass (80/20 wt%) exhibit higher storage modulus in comparison to pure PCL for frequencies between 0.01 Hz and 0.1 Hz.

Figs. 3 and 4 show the loss factor (tanδ) as a function of frequency for all blends at different temperatures. In all cases, results show that the loss factor decreases by increasing frequency indicating enhanced viscous behaviour or weakened elastic behaviour. Moreover, for all considered cases, it can be observed that the loss modulus decreases by increasing the deformation rate, which suggests that the elastic effect of the materials is becoming more important than their viscous effect, meaning that during the printing process the materials are becoming more viscous making them difficult to extrude through the nozzle. Furthermore, results show that for the same level of reinforcement the loss factor increases by increasing the temperature from 80 °C to 100 °C, as this temperature raise promotes a fluid-like behaviour making the materials easier to print. Additionally, for low frequencies and the same material content the loss factor decreases by increasing the material concentration, while by increasing the frequency rate this trend seems to disappear, suggesting that at high frequencies the material concentration effect is dominant compared to the deformation rate. For the same reinforcement concentration and temperature, PCL/TCP blends present higher loss factor value than PCL/HA and PCL/Bioglass blends, while PCL presents the higher loss factor. These results suggest that for the same level of reinforcement and processing parameters, PCL/TCP blends can be easily printed than PCL/HA and PCL/Bioglass blends.

3.3. *Cole-Cole plot analysis*

The Cole-Cole plot can be used to define the dispersion of a non-homogeneous material and the dielectric relaxation of polymer blends [65,66]. Moreover, through a Cole-Cole plot it is able to detect the relaxation time (τ_c) and zero shear viscosity (η_0) and the compatibility of the different materials in the blends [65–68]. Fig. 5 presents the semi quarter-circle plots for considered blends. Results show that the arc created from PCL/HA, PCL/TCP and PCL/Bioglass blends is larger compared to PCL, indicating that the relaxation time and zero shear viscosity of composite blends are higher, leading to longer re-orientation times and higher stresses during the printing process. Additionally, for the same bioceramic material by increasing the fillers concentration the elastic behaviour of the blends increases leading to the reduction of material flow during the printing process. In addition, results show that for the same material content, an increase in temperature reduces the arc, which becomes flatter, reducing the elasticity of the materials, indicating that the printing process is strongly determined by the viscous characteristics of the blends. Tables 2 and 3 present the zero-shear viscosity and relaxation time for the different blends at different temperatures. As observed the zero-shear viscosity increases by increasing the bioceramic content and decreases by increasing the temperature. The relaxation time depicts a similar trend. In addition, results show that for the same ceramic content and temperature, PCL/Bioglass blends present lower zero-shear viscosity, while PCL/TCP blends present lower relaxation time. In both cases PCL exhibits lower zero-shear viscosity and relaxation times than the polymer-ceramic blends.

3.4. *Rotational analysis*

Figs. 6 and 7 present the variation of the dynamic viscosity as a function of the shear rate for the different blends and different temperatures as a function of the shear rate. Based on these results it was possible to calculate the power law index (n) (Equation (4)) as shown in Table 4, which indicates that all blends exhibit a shear thinning behaviour being suitable for extrusion printing. Results show that at low shear rate values, PCL/HA, PCL/TCP and PCL/Bioglass blends present higher viscosity values than PCL. However, by increasing the shear rate up to a certain threshold value, the addition of ceramics and their concentration seems to have no major impact and a clear shear-thinning behaviour is observed for all considered samples [60–63,65,66,69,70]. Moreover, it is possible to observe that, for the same bioceramic content, the viscosity of the composite material increases with the concentration of the inorganic reinforcements. In the Newtonian region (flat plateau) the viscosity of the different blends decreases by increasing temperature, which can be attributed to an increase on the polymer chains movement [65,66,69,70]. Additionally, for the same ceramic material and the same temperature by increasing its concentration the dynamic viscosity is increasing. For the same material concentration and temperature, PCL/HA blends exhibit higher dynamic

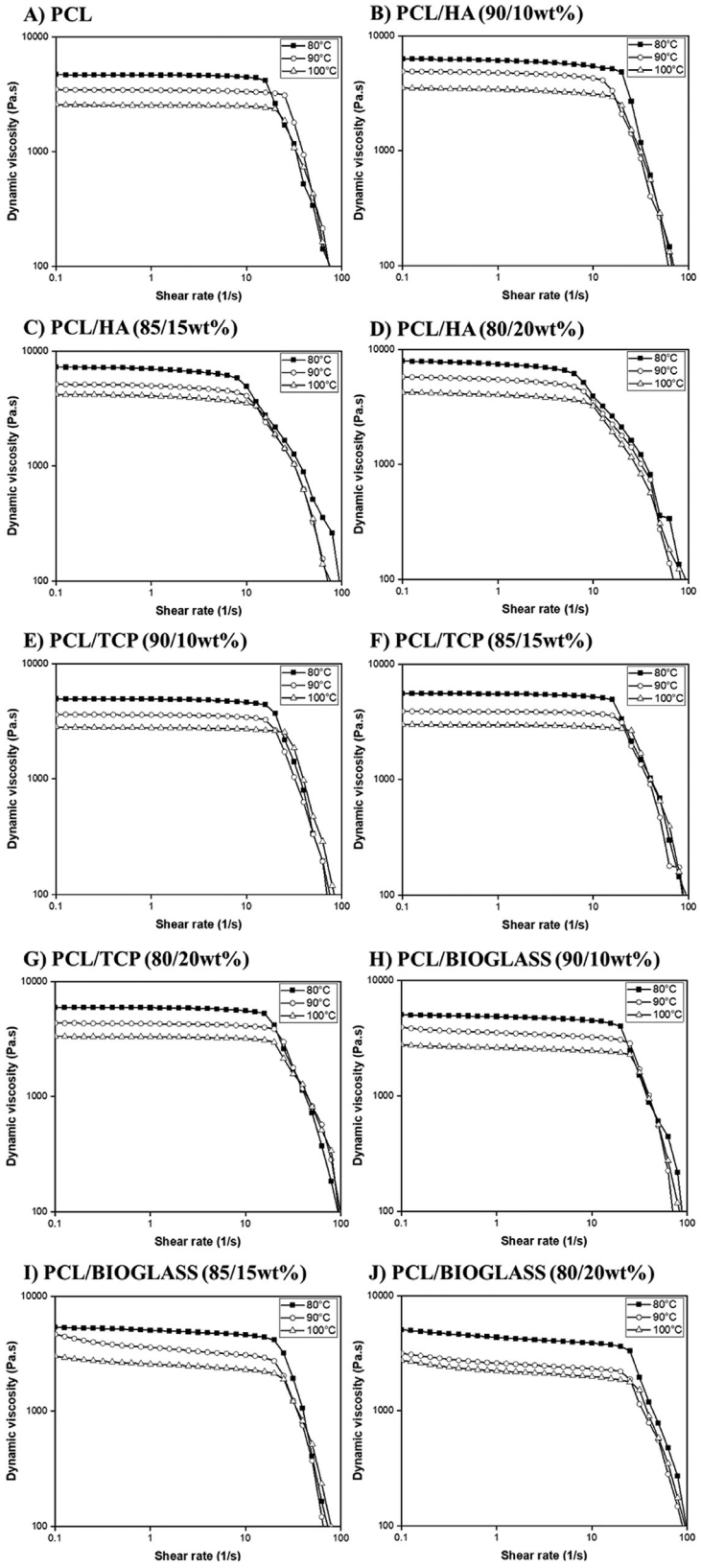

Fig. 6 – Shear rate as a function of dynamic viscosity for the same material concentration at different temperatures of A) PCL, B) PCL/HA (90/10 wt%), C) PCL/HA (85/15 wt%), D) PCL/HA (80/20 wt%), E) PCL/TCP (90/10 wt%), F) PCL/TCP (85/15 wt%), G) PCL/TCP (80/20 wt%), H) PCL/Bioglass (90/10 wt%), I) PCL/Bioglass (85/15 wt%) and J) PCL/Bioglass (80/20 wt%).

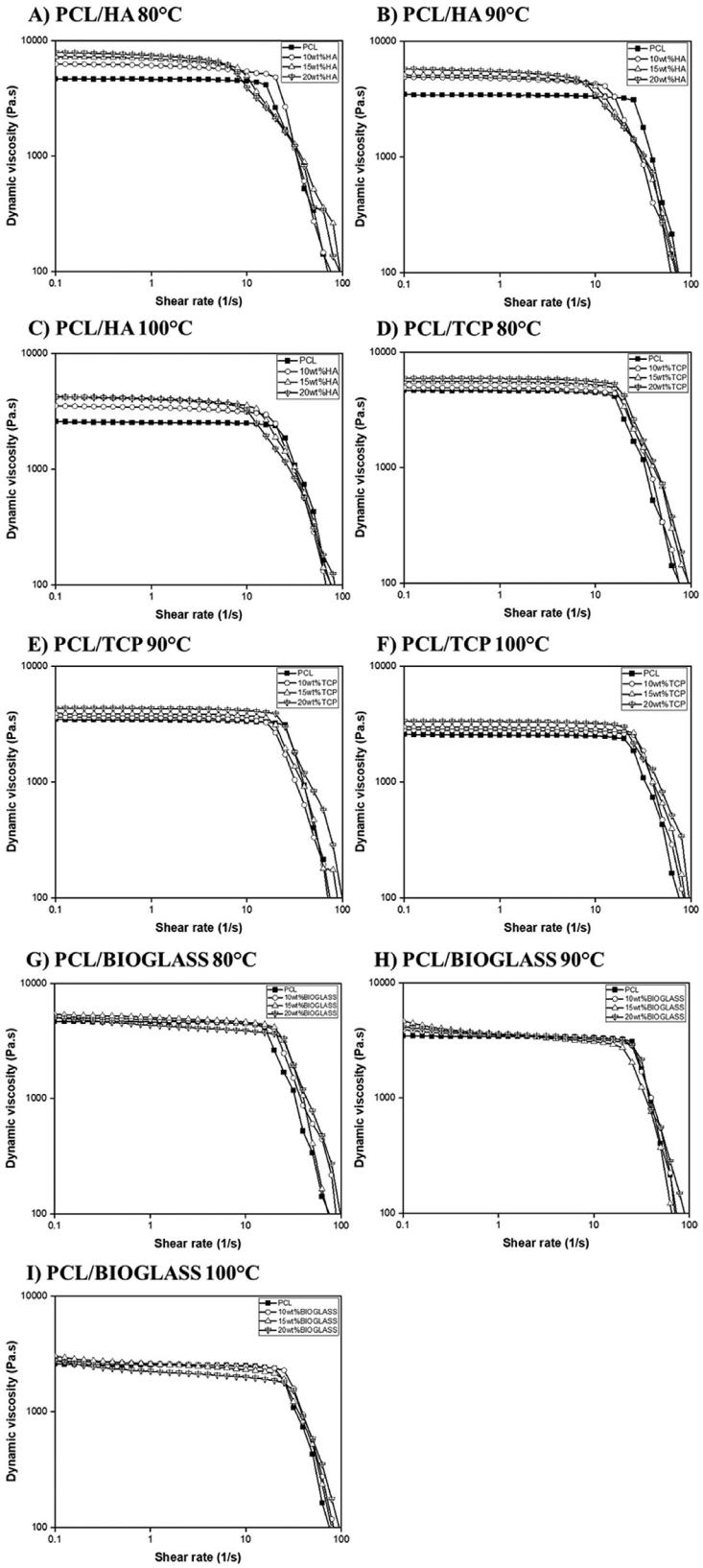

Fig. 7 – Shear rate as a function of dynamic viscosity for the same material content of A) PCL/HA (90/10 wt%), B) PCL/HA (85/15 wt%), C) PCL/HA (80/20 wt%), D) PCL/TCP (90/10 wt%), E) PCL/TCP (85/15 wt%), F) PCL/TCP (80/20 wt%), G) PCL/Bioglass (90/10 wt%), H) PCL/Bioglass (85/15 wt%) and I) PCL/Bioglass (80/20 wt%).

Table 4 – Power law index (n) and Adjusted (R2) results of polymer blends.

Temperature/Material Composition	80 °C	90 °C	100 °C
PCL	0.452	0.534	0.561
PCL/HA (90/10 wt%)	0.376	0.31	0.425
PCL/HA (85/15 wt%)	0.408	0.348	0.39
PCL/HA (80/20 wt%)	0.289	0.276	0.37
PCL/TCP (90/10 wt%)	0.455	0.452	0.617
PCL/TCP (85/15 wt%)	0.494	0.528	0.626
PCL/TCP (80/20 wt%)	0.508	0.629	0.681
PCL/Bioglass (90/10 wt%)	0.539	0.42	0.57
PCL/Bioglass (85/15 wt%)	0.413	0.258	0.478
PCL/Bioglass (80/20 wt%)	0.523	0.478	0.546

viscosity than PCL/TCP and PCL/Bioglass blends, while the lowest dynamic viscosity, between blends with the same ceramic concentration, was observed for PCL/Bioglass.

4. Conclusions

The viscoelastic properties of PCL and PCL-based composite blends (PCL/HA, PCL/TCP and PCL/Bioglass) containing different levels of reinforcements (10 wt%, 15 wt% and 20 wt%) was investigated to determine the suitability of these blends for screw-assisted extrusion-based additive manufacturing. At low frequencies all blends present higher viscous modulus than elastic modulus, but these differences tend to reduce by increasing the frequency values. Moreover, the addition of ceramic materials increases both viscous modulus and elastic modulus. Moreover, PCL/HA present higher elastic modulus than PCL/TCP and PCL/Bioglass ones. Composite blends also exhibit longer relaxation times compared with PCL. Overall, for the same material concentration and temperature, blends containing Bioglass particles present slightly lower elastic modulus than PCL/HA blends, and lower loss factor, relaxation times and shear viscosities than PCL, PCL/HA and PCL/TCP, indicating that PCL/Bioglass blends are more suitable and easier to handle during the printing process.

Author contributions

Conceptualization, E.D. and P.B.; methodology, E.D., M.H.H. and A.M.O.; software, E.D; validation, E.D., M.H.H, A.M.O. and P.B.; formal analysis, E.D. and P.B.; investigation, E.D., M.H.H., A.M.O. and P.B.; resources, All Authors.; data curation, All Authors; writing—original draft preparation, E.D.; writing—review and editing, All Authors; visualization, E.D. and P.B.; supervision, G.C, A.W. and P.B.; project administration, P.B.; funding acquisition, P.B. All authors have read and agreed to the published version of the manuscript.

Funding

This project has been supported by the University of Manchester and the Engineering and Physical Sciences Research Council (EPSRC) of the UK, the Global Challenges Research Fund (GCRF), grant number EP/R01513/1.

Declaration of competing interest

The authors declare the following financial interests/personal relationships which may be considered as potential competing interests. Evangelos Daskalakis reports financial support was provided by Engineering and Physical Sciences Research Council.

Acknowledgments

The authors would like to thank the support received from both the University of Manchester and the Engineering and Physical Sciences Research Council (EPSRC) of the UK. This manuscript is the result of the work completed by Evangelos Daskalakis toward a Ph.D. in Mechanical Engineering, granted by the University of Manchester in September of 2022.

REFERENCES

[1] Donate R, Monzón M, Alemán-Domínguez M. Additive manufacturing of PLA-based scaffolds intended for bone regeneration and strategies to improve their biological properties. E-Polymers 2020;20(1):571–99.
[2] Roque R, Barbosa G, Guastaldi A. Design and 3D bioprinting of interconnected porous scaffolds for bone regeneration. An additive manufacturing approach. J Manuf Process 2021;64:655–63.
[3] Chen Y, Li W, Zhang C, Wu Z, Liu J. Recent developments of biomaterials for additive manufacturing of bone scaffolds. Advanced Healthcare Materials 2020;9(23):2000724.
[4] Qu H. Additive manufacturing for bone tissue engineering scaffolds. Mater Today Commun 2020;24:101024.
[5] Garot C, Bettega G, Picart C. Additive manufacturing of material scaffolds for bone regeneration: toward application in the clinics. Adv Funct Mater 2020;31(5):2006967.
[6] Wu H, Fahy W, Kim S, Kim H, Zhao N, Pilato L, et al. Recent developments in polymers/polymer nanocomposites for additive manufacturing. Prog Mater Sci 2020;111:100638.
[7] Krauel L, Valls-Esteve A, Tejo-Otero A, Fenollosa-Artés F. 3D-Printing in surgery: beyond bone structures. A review. Annals of 3D Printed Medicine 2021;4:100039.
[8] Sherborne C, Owen R, Reilly G, Claeyssens F. Light-based additive manufacturing of PolyHIPEs: controlling the surface porosity for 3D cell culture applications. Mater Des 2018;156:494–503.
[9] Zhou Z, Lennon A, Buchanan F, McCarthy H, Dunne N. Binder jetting additive manufacturing of hydroxyapatite powders: effects of adhesives on geometrical accuracy and green compressive strength. Addit Manuf 2020;36:101645.
[10] Ahn J, Kim J, Han G, Kim D, Cheon K, Lee H, et al. 3D-printed biodegradable composite scaffolds with significantly enhanced mechanical properties via the combination of binder jetting and capillary rise infiltration process. Addit Manuf 2021;41:101988.
[11] Yang J, Jin X, Gao H, Zhang D, Chen H, Zhang S, et al. Additive manufacturing of trabecular tantalum scaffolds by laser powder bed fusion: mechanical property evaluation and

porous structure characterization. Mater Char 2020;170:110694.
[12] McGregor M, Patel S, McLachlin S, Mihaela V. Architectural bone parameters and the relationship to titanium lattice design for powder bed fusion additive manufacturing. Addit Manuf 2021;47:102273.
[13] Beheshtizadeh N, Azami M, Abbasi H, Farzin A. Applying extrusion-based 3D printing technique accelerates fabricating complex biphasic calcium phosphate-based scaffolds for bone tissue regeneration. J Adv Res 2021;0:1–26.
[14] Pierantozzi D, Scalzone A, Jindal S, Stɒniece L, Šalma-Ancāne K, Dalgarno K, et al. 3D printed Sr-containing composite scaffolds: effect of structural design and material formulation towards new strategies for bone tissue engineering. Compos Sci Technol 2020;191:108069.
[15] Borkar T, Goenka V, Jaiswal A. Application of poly-ε-caprolactone in extrusion-based bioprinting. Bioprinting 2021;21:e00111.
[16] Kolan KC, Huang YW, Semon JA, Leu MC. 3D-printed biomimetic bioactive glass scaffolds for bone regeneration in rat calvarial defects. International Journal of Bioprinting 2020;6(2):274.
[17] Wang F, Tankus E, Santarella F, Rohr N, Sharma N, Märtin S, et al. Fabrication and characterization of PCL/HA filament as a 3D printing material using thermal extrusion technology for bone tissue engineering. Polymers 2022;14(4):669.
[18] Cestari F, Petretta M, Yang Y, Motta A, Grigolo B, Sglavo V. 3D printing of PCL/nano-hydroxyapatite scaffolds derived from biogenic sources for bone tissue engineering. Sustainable Mater Technol 2021;29:e00318.
[19] Tümer E, Erbil H. Extrusion-based 3D printing applications of PLA composites: a review. Coatings 2021;11(4):390.
[20] Manzoor F, Golbang A, Jindal S, Dixon D, McIlhagger A, Harkin-Jones E, et al. 3D printed PEEK/HA composites for bone tissue engineering applications: effect of material formulation on mechanical performance and bioactive potential. J Mech Behav Biomed Mater 2021;121:104601.
[21] Choi E, Kim D, Kang D, Yang GH, Jung B, Yeo M, et al. 3D-printed gelatin methacrylate (GelMA)/silanated silica scaffold assisted by two-stage cooling system for hard tissue regeneration. Regenerative Biomaterials 2021;8(2):rbab001.
[22] Sinha R, Sanchez A, Camara-Torres M, Uriszar-Aldaca I, Calore A, Harings J, et al. Additive manufactured scaffolds for bone tissue engineering: physical characterization of thermoplastic composites with functional fillers. ACS Applied Polymer Materials 2021;3(8):3788–99.
[23] Du C, Hu J, Wu X, Shi H, Yu H, Qian J, et al. 3D printing of a tough double-network hydrogel and its use as a scaffold to construct a tissue-like hydrogel composite. J Mater Chem B 2022;10(3):468–76.
[24] Mondal D, Srinivasan A, Comeau P, Toh Y, Willett T. Acrylated epoxidized soybean oil/hydroxyapatite-based nanocomposite scaffolds prepared by additive manufacturing for bone tissue engineering. Mater Sci Eng C 2021;11:111400.
[25] Jeyachandran P, Bontha S, Bodhak S, Balla V, Doddamani M. Material extrusion additive manufacturing of bioactive glass/high density polyethylene composites. Compos Sci Technol 2021;213:108966.
[26] Betancourt N, Chen X. Review of extrusion-based multi-material bioprinting processes. Bioprinting 2022;25:e00189.
[27] Dixit K, Sinha N. Additive manufacturing of carbon nanotube reinforced bioactive glass scaffolds for bone tissue engineering. J Eng Sci Med Diagnostics Therapy 2021;4(4):41004–11.
[28] Diaz-Gomez L, Elizondo M, Kontoyiannis P, Koons G, Dacunha-Marinho B, Zhang X, et al. Three-dimensional extrusion printing of porous scaffolds using storable ceramic inks. Tissue Eng C Methods 2020;26(6):292–305.
[29] Shao H, Wu J, Wang S, Duan J, Zhang Y, Peng J, et al. 3D gel-printing of porous MgFe2O4 magnetic scaffolds for bone tissue engineering. Ceram Int 2022;48(5):7183–91.
[30] Zhang W, Ullah I, Shi L, Zhang Y, Ou H, Zhou J, et al. Fabrication and characterization of porous polycaprolactone scaffold via extrusion-based cryogenic 3D printing for tissue engineering. Mater Des 2019;180:107946.
[31] Abouzeid R, Khiari R, Beneventi D, Dufresne A. Biomimetic mineralization of three-dimensional printed alginate/TEMPO-oxidized cellulose nanofibril scaffolds for bone tissue engineering. Biomacromolecules 2018;19(11):4442–52.
[32] Hernández-González A, Téllez-Jurado L, Rodríguez-Lorenzo L. Alginate hydrogels for bone tissue engineering, from injectables to bioprinting: a review. Carbohydrate Polymers. 3030; 229; 115514.
[33] Chen G, Chen N, Wang Q. Fabrication and properties of poly(vinyl alcohol)/β-tricalcium phosphate composite scaffolds via fused deposition modeling for bone tissue engineering. Compos Sci Technol 2019;172:17–28.
[34] Hu T, Cui X, Zhu M, Wu M, Tian Y, Yao B, et al. 3D-printable supramolecular hydrogels with shear-thinning property: fabricating strength tunable bioink via dual crosslinking. Bioact Mater 2020;5(4):808–18.
[35] Chen Y, Xiong X, Liu X, Cui R, Wang C, Zhao G, et al. 3D Bioprinting of shear-thinning hybrid bioinks with excellent bioactivity derived from gellan/alginate and thixotropic magnesium phosphate-based gels. J Mater Chem B 2020;8(25):5500–14.
[36] Zandi N, Sani E, Mostafavi E, Ibrahim D, Saleh B, Shokrgozar M, et al. Nanoengineered shear-thinning and bioprintable hydrogel as a versatile platform for biomedical applications. Biomaterials 2021;267:120476.
[37] Vishnurajan P, Karuppudaiyan S, Singh DKJ. Design and analysis of feature primitive scaffold manufactured using 3D-printer—fused deposition modelling (FDM). Lecture Notes in Mechanical Engineering 2020:577–88.
[38] Esposito Corcione C, Gervaso F, Scalera F, Padmanabhan S, Madaghiele M, Montagna F, et al. Highly loaded hydroxyapatite microsphere/PLA porous scaffolds obtained by fused deposition modelling. Ceram Int 2019;45(2):2803–10.
[39] Justino Netto J, Idogava H, Frezzatto Santos L, Silveira Z, Romio P, Alves J. Screw-assisted 3D printing with granulated materials: a systematic review. Int J Adv Des Manuf Technol 2021;115:2711–27.
[40] Criado-Gonzalez M, Dominguez-Alfaro A, Lopez-Larrea N, Alegret N, Mecerreyes D. Additive manufacturing of conducting polymers: recent advances, Challenges, and opportunities. ACS Appl Polymer Mater 2021;3(6):2865–83.
[41] Maia F, Bastos A, Oliveira J, Correlo V, Reis R. Recent approaches towards bone tissue engineering. Bone 2022;154:116256.
[42] Dalavi PA, Anil S, Venkatesan J. Bioceramics-based biomaterials for bone tissue engineering. Eng Mater Stem Cell Regener 2021:573–87.
[43] Naidu N, Wadher K, Umekar M. An overview on biomaterials: pharmaceutical and biomedical applications. J Drug Deliv Therapeut 2021;11(1-s):154–61.
[44] Sharifi F, Atyabi S, Norouzian D, Zandi M, Irani S, Bakhshi H. Polycaprolactone/carboxymethyl chitosan nanofibrous scaffolds for bone tissue engineering application. Int J Biol Macromol 2018;115:243–8.
[45] Teoh S, Goh B, Lim J. Three-dimensional printed polycaprolactone scaffolds for bone regeneration success and future perspective. Tissue Eng 2019;25(13–14):931–5.

[46] Wasyłeczko M, Sikorska W, Chwojnowski A. Review of synthetic and hybrid scaffolds in cartilage tissue engineering. Membranes 2020;10(11):348.
[47] Ilyas R, Zuhri M, Norrrahim M, Misenan M, Jenol M, Samsudin S, et al. Natural fiber-reinforced polycaprolactone green and hybrid biocomposites for various advanced applications. Polymers 2022;14(1):182.
[48] Chen C, Chen S, Lin S, Liang H, Wu C. Clinical efficacy of polycaprolactone β-calcium triphosphate composite for osteoconduction in rabbit bone defect model. Polymers 2021;13(15):2552.
[49] Zhao J, Guo L, Yang X, Weng J. Preparation of bioactive porous HA/PCL composite scaffolds. Appl Surf Sci 2008;255(5):2942–6.
[50] Kim Y, Lim J, Yang G, Seo J, Ryu H, Kim G. 3D-printed PCL/bioglass (BGS-7) composite scaffolds with high toughness and cell-responses for bone tissue regeneration. J Ind Eng Chem 2019;79:163–71.
[51] Gatto M, Furlani M, Giuliani A, Bloise N, Fassina L, Visai L, et al. Biomechanical performances of PCL/HA micro- and macro-porous lattice scaffolds fabricated via laser powder bed fusion for bone tissue engineering. Mater Sci Eng C 2021;128:112300.
[52] Simorgh S, Alasvand N, Khodadadi M, Ghobadi F, Malekzadeh KM, Brouki MP, Kargozar S, Baino F, Mobasheri A, Mozafari M. Additive manufacturing of bioactive glass biomaterials. Methods 2022;208:75–91.
[53] Tan G, Wang W, Cheng Y, Wang Y, Zhu Z. Master curve establishment and complex modulus evaluation of SBS-modified asphalt mixture reinforced with basalt fiber based on generalized sigmoidal model. Polymers 2020;12(7):1586.
[54] Poslinski A, Ryan M, Gupta R, Seshadri S, Frechette F. Rheological behavior of filled polymeric systems I. Yield stress and shear-thinning effects. J Rheol 1998;32(7):703–35.
[55] Gerdes S, Mostafavi A, Ramesh S, Memic A, Rivero I, Rao P, et al. Process–structure–quality relationships of three-dimensional printed poly(caprolactone)-hydroxyapatite scaffolds. Tissue Eng 2020;26(5–6):279–91.
[56] Oryan A, Hassanajili S, Sahvieh S. Effectiveness of a biodegradable 3D polylactic acid/poly(ϵ-caprolactone)/hydroxyapatite scaffold loaded by differentiated osteogenic cells in a critical-sized radius bone defect in rat. J Tissue Eng Regenerative Med 2020;15(2):150–62.
[57] Mohd Pu'ad N, Abdul Haq R, Mohd Noh H, Abdullah H, Idris M, Lee T. Review on the fabrication of fused deposition modelling (FDM) composite filament for biomedical applications. Mater Today Proc 2020;29:228–32.
[58] Beatrice C, Shimomura K, Backes E, Harb S, Costa L, Passador F, et al. Engineering printable composites of poly (ε-polycaprolactone)/β-tricalcium phosphate for biomedical applications. Polym Compos 2020;42(3):1198–213.
[59] Hajiali F, Tajbakhsh S, Shojaei A. Fabrication and properties of polycaprolactone composites containing calcium phosphate-based ceramics and bioactive glasses in bone tissue engineering: a review. Polym Rev 2017;58(1):164–207.
[60] Fernandes H, Gaddam A, Rebelo A, Brazete D, Stan G, Ferreira J. Bioactive glasses and glass-ceramics for healthcare applications in bone regeneration and tissue engineering. Materials 2018;11(12):2530.
[61] Deliormanlı A, Konyalı R. Bioactive glass/hydroxyapatite-containing electrospun poly (ε-Caprolactone) composite nanofibers for bone tissue engineering. J Aust Ceramic Soc 2018;55(1):247–56.
[62] Huang B, Bártolo P. Rheological characterization of polymer/ceramic blends for 3D printing of bone scaffolds. Polym Test 2018;68:365–78.
[63] Hassanajili S, Karami-Pour A, Oryan A, Talaei-Khozani T. Preparation and characterization of PLA/PCL/HA composite scaffolds using indirect 3D printing for bone tissue engineering. Mater Sci Eng C 2019;104:109960.
[64] Poh P, Hutmacher D, Stevens M, Woodruff M. Fabrication and in vitro characterization of bioactive glass composite scaffolds for bone regeneration. Biofabrication 2013;5(4):045005.
[65] Ahmed J, Auras R, Kijchavengkul T, Varshney S. Rheological, thermal and structural behavior of poly(ε-caprolactone) and nanoclay blended films. J Food Eng 2012;111(4):580–9.
[66] Ahmed J, Varshney S, Auras R. Rheological and thermal properties of polylactide/silicate nanocomposites films. J Food Sci 2010;75(2):N17–24.
[67] Dong R, Pang Y, Su Y, Zhu X. Supramolecular hydrogels: synthesis, properties and their biomedical applications. Biomater Sci 2015;3(7):937–54.
[68] Gulrez S, Al-Assaf S, Fang Y, Phillips G, Gunning A. Revisiting the conformation of xanthan and the effect of industrially relevant treatments. Carbohydrate Polymers 2012;90(3):1235–43.
[69] De Almeida J, Da Silva A, Escócio V, Da Fonseca Thomé Da Silva A, De Sousa A, Nascimento C, et al. Rheological, mechanical and morphological behavior of polylactide/nano-sized calcium carbonate composites. Polym Bull 2016;73(12):3531–45.
[70] López Manchado M, Biagiotti J, Kenny J. Rheological behavior and processability of polypropylene blends with rubber ethylene propylene diene terpolymer. J Appl Polym Sci 2001;81(1):1–10.